THE JOURNAL OF PHYSICAL CHEMISTRY A

Article

pubs.acs.org/JPCA

Intramolecular Charge Transfer and Solvation Dynamics of Thiolate-Protected $Au_{20}(SR)_{16}$ Clusters Studied by Ultrafast Measurement

Meng Zhou,[†] Silvije Vdović,[†,‡] Saran Long,[†] Manzhou Zhu,[§] Linyin Yan,[†] Yingying Wang,[†] Yingli Niu,[†] Xuefei Wang,[†] Qianjin Guo,*[,†] Rongchao Jin,*[,§] and Andong Xia*[,†]

[†]The State Key Laboratory of Molecular Reaction Dynamics and Beijing National Laboratory for Molecular Sciences (BNLMS), Institute of Chemistry, Chinese Academy of Sciences, Beijing 100190, People's Republic of China

[‡]Institute of Physics, Bijenička cesta 46, 10000 Zagreb, Croatia

[§]Department of Chemistry, Carnegie Mellon University, 4400 Fifth Avenue, Pittsburgh, Pennsylvania 15213, United States

Supporting Information

ABSTRACT: It is accepted that the monolayer ligand shell in monolayer-protected gold nanoclusters (MPCs) plays an important role in stabilizing the metal core structure. Previous reports have shown that the core and shell do not interact chemically, and very few studies investigating the intramolecular charge transfer (ICT) between the core and ligand shell in clusters have been reported. The underlying excited state relaxation mechanisms about the influence of solvents, the optically excited vibration, and the roles of the core and shell in charge transfer remain unknown to a large extent. Here we report a femtosecond transient absorption study of a $Au_{20}(SR)_{16}$ (R = CH_2CH_2Ph) cluster in toluene and tetrahydrofuran. The ICT from the outside shell to the inside core upon excitation in $Au_{20}(SR)_{16}$ is identified. The observed solvation-dependent oscillations in different solvents further confirm the photoinduced ICT formation in $Au_{20}(SR)_{16}$. The results provide a fundamental understanding of the structure−property relationships about the solvation-dependent core−shell interaction in Au MPCs.

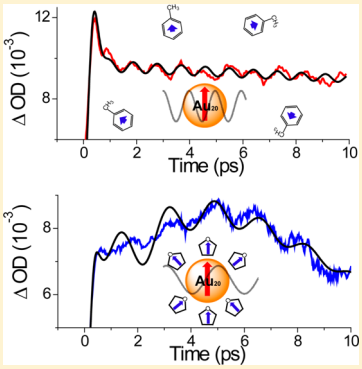

INTRODUCTION

Monolayer-protected Au clusters have attracted considerable attention in terms of both understanding the fundamental science[1,2] and potential applications in a number of areas, such as catalysis,[3,4] biolabeling,[5] and optics.[6−8] The ability to modify electronic and optical properties by synthesizing Au clusters with precise numbers of Au atoms and ligands is very important for the development of their wide applications.[9,10] Metal particles exhibit new properties because of quantum confinement effects when their sizes approach the electron's Fermi wavelength. With a diameter of <2 nm, gold clusters start to show discrete molecular-like optical transitions and enhanced near-infrared (NIR) luminescence,[8,11] which are distinct indications of the transition from metallic to semiconducting behavior.[12] To gain a deeper understanding of the correlation between electronic properties and cluster structure, investigations of the excited state dynamics of Au clusters with well-defined structure are fundamentally important.[13−15]

Small Au nanoparticles (<2 nm) or clusters act like superatoms,[16,17] with no surface plasmon resonance (SPR) band appearing in their steady state absorption spectra.[15,18] Investigations of the dynamics of Au clusters can elucidate details of the influence of electronic structure and geometry on the properties of these very small Au particles with a quantum confinement effect.[19,20] With the aid of femtosecond pump−probe techniques, a core−shell relaxation model was proposed in relaxation dynamics of small clusters (for example, Au_{25}) where fast internal conversion and slow internal conversion were assigned to transitions between core states and transitions from the core to the shell state, respectively.[13] The oscillatory features were observed in their transient kinetic traces of Au_{25} clusters, resulting from excitation of the Au core's radial breathing modes,[13] which modulate excited state transitions of the clusters. Meanwhile, a displacive excitation mechanism that deviated from the elastic sphere model was also introduced to explain the oscillations in quantum-sized Au clusters.[21,22]

The monolayer ligand shell in protected clusters plays an important role in stabilizing the metal core structure.[2] Previous reports have shown that the core and shell do not interact chemically, and very few studies of the intramolecular charge transfer (ICT) between the core and ligands shell in monolayer-protected Au clusters have been reported,[23] although the dual fluorescence was observed, where the NIR emission possibly originated from the interaction between the metal core and the outer ligand (thiolate) shell.[8,24] It is known that the nature of optical excitation and the degree of ICT are strongly influenced by geometric confinement and charge symmetry as well as their surrounding environments.[25] Once these clusters are excited to highly excited states, the excess energy is expected to be transferred to the surrounding medium

Received: June 26, 2013
Revised: September 15, 2013
Published: September 17, 2013

   dx.doi.org/10.1021/jp406336q | J. Phys. Chem. A 2013, 117, 10294−10303

during the relaxation in which solvents are involved. Thus, the solvent molecules could play an important role in the excited state relaxation of Au clusters, where the oscillatory features could be affected by the response in dynamics of the solvent molecules to photoinduced charge redistribution of the excited Au clusters. Overall, the underlying excited state relaxation mechanisms about the influence of solvents, the origin of the optically excited vibration, and the roles of the core and shell in charge transfer of Au clusters remain unknown to a large extent.

In this article, we report a broadband femtosecond transient absorption study of the $Au_{20}(SR)_{16}$ (R = CH_2CH_2Ph) cluster in toluene and tetrahydrofuran (THF). The structure of $Au_{20}(SR)_{16}$ was predicted to possess an Au_8 inner core (or kernel) protected by "staplelike" surface motifs (Figure 1).[25,26]

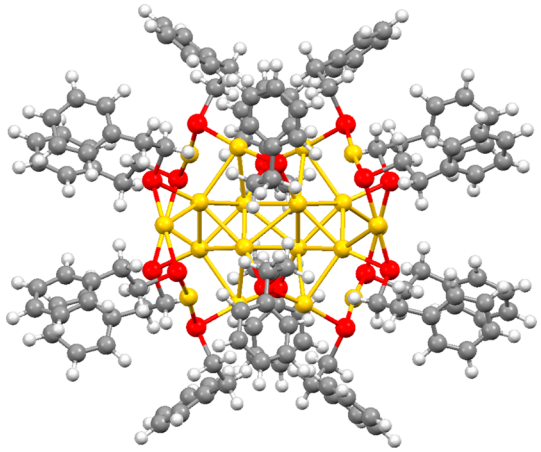

Figure 1. Theoretical predicted structure of $Au_{20}(SCH_2CH_2Ph)_{16}$. Au atoms are colored yellow, S atoms red, C atoms gray, and H atoms: light gray.

As the $PhCH_2CH_2$ group has the ability to donate electron densities,[24] the ligands in $Au_{20}(SR)_{16}$ are more likely to act as electron density donors, where the Au_8 core acts as an acceptor. Our quantum chemical calculations of charge difference density (CDDs) of $Au_{20}(SR)_{16}$ predict the presence of intramolecular charge transfer (ICT) character of the excited state, whereupon excitation the charge transfers from the outside shell to the inside core. The ICT state and sequentially solvent-stabilized and relaxed ICT (named ICT′ to differentiate it from ICT) state are further observed in the pump−probe measurements, where the relaxed ICT′ state is more pronounced in more polar THF than in less polar toluene. The solvent-dependent oscillations of the excited $Au_{20}(SR)_{16}$ cluster are identified, and the obvious discrepancy in oscillation frequency in polar THF versus less polar toluene originates from the increased mass of the oscillator, where the more polar THF molecules closely approach the excited $Au_{20}(SR)_{16}$ cluster surface forming a single layer solvent shell due to solvation, leading to the reduced oscillation frequency. The mass and number of THF molecules absorbed around the excited $Au_{20}(SR)_{16}$ cluster surface can be further semiquantitatively estimated according to the oscillation frequency shift relative to that in toluene. The observed solvation-dependent oscillations may possibly act as a solvent mass sensor that may stimulate more related applications in the future. The detailed photophysical properties of excited $Au_{20}(SR)_{16}$ cluster relaxation provide a fundamental understanding of the structure−property relationships in gold monolayer-protected clusters, where the solvent effects and dynamics of the ICT state-dependent oscillations could be important parameters for understanding the complicated spectral properties with different surrounding environments.

MATERIALS AND METHODS

Materials. The synthesis of the $Au_{20}(SR)_{16}$ cluster by Jin and co-workers was reported previously.[26] For the spectroscopic measurements, purified $Au_{20}(SR)_{16}$ (stored in powder form in a dry and dark container) was dissolved in proper solvents (i.e., toluene and tetrahydrofuran, both of AR grade).

Steady State Spectroscopy. Ultraviolet−visible (UV−vis) absorption and fluorescence spectra were recorded on a UV1601 spectrometer (UV1601, Shimadzu) and a fluorescence spectrometer (F4500, Hitachi), respectively, at ambient temperature.

Femtosecond Transient Absorption Measurements. The femtosecond transient absorption was measured using a home-built femtosecond broadband pump−probe setup. Briefly, a regeneratively amplified Ti:sapphire laser (Coherent Legend Elite) produces 40 fs, 1 mJ pulses at a 500 Hz repetition rate at 800 nm with a bandwidth (FWHM) of ∼30 nm. The output from the amplifier is split by a 90/10 beamsplitter to generate pump and probe beams. A portion of the 800 nm pulse was doubled with a 0.5 mm thick BBO (type I) crystal to provide the 400 nm pump pulse. The probe beam at 800 nm was sent to a computer-controlled optical delay line and then focused onto a 2 mm thick water cell to generate a white light continuum that was split into two beams using a broadband 50/50 beamsplitter as the reference and signal beams. The focused signal and pump beams were overlapped into a flow cell with a 1 mm beam path length, and the reference beam passed through the unexcited part of the sample. Signal and reference beams were detected on a fiber-coupled dual-channel spectrometer (Avantes AvaSpec-2048-2-USB2). For each pump pulse, spectral intensities of the signal and the reference without excitation of the sample (I^{off}_{probe} and I^{off}_{ref}, respectively) and in the presence of the pump (I^{on}_{probe} and I^{on}_{ref}, respectively) are measured. The transient absorption difference signal (for a given time delay) can be calculated from the following formula:

$$\Delta OD(t, \lambda) = -\log\left[\frac{I^{on}_{probe}(t, \lambda)}{I^{off}_{probe}(t, \lambda)} \times \frac{I^{off}_{ref}(t, \lambda)}{I^{on}_{ref}(t, \lambda)}\right]$$

Every spectrum is recorded 200 times, and the averaged spectrum is used in further data processing. The concentration of the sample was adjusted to an absorbance of 0.3 OD at 400 nm in a 1 mm path length quartz cuvette. No photodegradation was observed after femtosecond transient absorption measurements. To measure isotropic signals, the mutual polarizations of pump and probe beams were set to the magic angle (54.7°) using a half-wave plate.

Data Analysis. The differential absorbance $\Delta A(t,\lambda)$ as a function of wavelength and time delay was analyzed using the population dynamics modeling toolbox software developed by van Wilderen et al.[27] Spectral chirp in the transient absorption spectra was corrected for group velocity dispersion of the probe beam. A sequential decay pathway was utilized to model the $\Delta A(t,\lambda)$ data, which is a superposition of different spectral components, $\varepsilon_l(\lambda)$, weighted by their concentration, $c_l(t)$:[28]

dx.doi.org/10.1021/jp406336q | J. Phys. Chem. A 2013, 117, 10294−10303

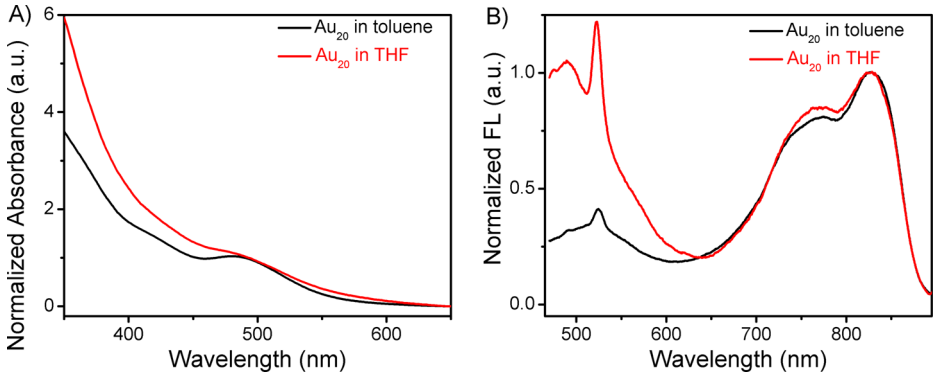

Figure 2. Normalized steady state spectra of the $Au_{20}(SR)_{16}$ cluster. (A) Steady state absorption and (B) fluorescence spectra of the $Au_{20}(SR)_{16}$ cluster in toluene and THF. The spike at ~520 nm observed in both solvents is proved to be Raman scattering of the solvent by measuring fluorescence with neat solvent (see Figure S1 of the Supporting Information).

$$\Delta A(t, \lambda) = \sum_{l=1}^{n} c_l(t)\varepsilon_l(\lambda)$$

A sequential scheme with increasing lifetimes is used, resulting in evolution-associated difference spectra (EADS). The Fourier transform of the kinetic data at a specific wavelength was calculated to obtain the frequency of the acoustic vibration. The amplitude of the Fourier transform is determined by calculating the value around the peak of the vibration mode.

Quantum Chemical Calculations. The quantum chemical calculations on the $Au_{20}(SR)_{16}$ cluster were based on the structure obtained from Pei's work. For computing efficiency, the -R group was substituted with $-CH_3$. The stable ground state geometry of $Au_{20}(SR)_{16}$ was optimized using the PBE[29] function with the LANL2DZ basis set for Au and the 6-31G(d,p) basis set for S, C, and H. The vibrational frequency calculations and the single-point calculations were performed on the optimal geometry. The single-point calculations of the excited states of $Au_{20}(SR)_{16}$ were computed by the time-dependent density functional theory (TD-DFT) at the same level and basis. The charge difference density (CDDs) cube was constructed on the basis of the single-point calculations of the ground state and the excited state. All the calculations were conducted by the method implemented in the Gaussian 03 program package.[30]

RESULTS AND DISCUSSION

Steady State Absorption and Fluorescence Spectra. Figure 2 shows the steady state absorption and fluorescence spectra of $Au_{20}(SR)_{16}$ dissolved in toluene and tetrahydrofuran, respectively. The extremely small size of the $Au_{20}(SR)_{16}$ cluster (Au_8 core size of ~0.66 nm and overall size of $Au_{20}(SR)_{16}$ of ~0.98 nm estimated according to quantum chemical optimization) leads to strong quantum confinement of electrons in the particle, resulting in a stepwise multiband absorption spectrum as well as a large band gap of 2.15 eV for $Au_{20}(SR)_{16}$. In toluene, the strong absorption peak around 485 nm is assigned to the HOMO−LUMO transition, whereas the broad peaks around 420 and 350 nm are identified as transitions between HOMO − n and LUMO + n. Besides, these three bands are attributed to interband transition from the 5d to 6sp orbital of $Au_{20}(SR)_{16}$.[31] These peaks are somewhat broadened in more polar THF than in toluene because of the increased level of polarization. As the electronic structure of clusters mainly depends on their core structures,[14,15,31] it is found that the linear absorption spectrum of $Au_{20}(SR)_{16}$ with a prolate Au_8 inner core differs largely from that of Au_{25} whose core is nearly spherical.[32]

The steady state emission of $Au_{20}(SR)_{16}$ in both solvents when it is excited at 450 nm is extremely weak and shows broad bands in both NIR and visible regions. We found that the NIR luminescence of $Au_{20}(SR)_{16}$ in both solvents shows two peaks around 770 nm (1.61 eV) and 820 nm (1.51 eV), which are subgap emissions and ascribed to intraband transitions arising from recombination of surface-trapped carriers.[33] Meanwhile, the visible luminescence, possibly resulting directly from the HOMO−LUMO transition, is effectively enhanced relative to the NIR emission in THF compared to that in toluene, the origin of which remains to be elucidated. It is possible that the visible emission mainly depends on the core structure, where a more polar environment in THF could induce a polarization to the clusters to affect the emission of clusters. The observed dual fluorescence is a typical indicator of the charge transfer occurring in $Au_{20}(SR)_{16}$ upon excitation.[24] As the $PhCH_2CH_2$ group has the ability to donate electron densities,[24] the ligands in $Au_{20}(SR)_{16}$ are more likely to act as electron density donors. To gain deeper insight into the nature of the ICT state, we performed the following charge difference density (CDD) calculations according to refs 34−37, where CDD means the difference in electron density upon the electronic transition between the ground and excited states.

Visualized Charge Difference Density. To verify the charge transfer pathway and local excited character of transitions in the $Au_{20}(SR)_{16}$ cluster, the visualized CDD based on TD-DFT methods as implemented in the Gaussian 03 package[30] was calculated. The methods and basis sets were chosen according to the work by Pei et al.,[31] and details of the calculation are provided in Figure S5 of the Supporting Information. The CDD visualized the difference in electron density upon excitation between the ground state and the excited states.[34−37] The calculated absorption spectrum based on TD-DFT is shown in Figure 3, where the peaks at 2.75 and 2.97 eV are in good agreement with the experiment (Figure 2A) and simulation from previous work.[31] Besides, the band edge based on the calculated results is 2.25 eV, very close to the experimental value of 2.15 eV.[26] The inset of Figure 3 shows the visualized CDD of the S_1-S_0 transition upon excitation, presenting direct evidence of intramolecular charge transfer (ICT) from outside ligands to the inner metal core, where the four $Au_3(SR)_4$ semirings act as donors and the Au_8 core acts as

dx.doi.org/10.1021/jp406336q | J. Phys. Chem. A 2013, 117, 10294−10303

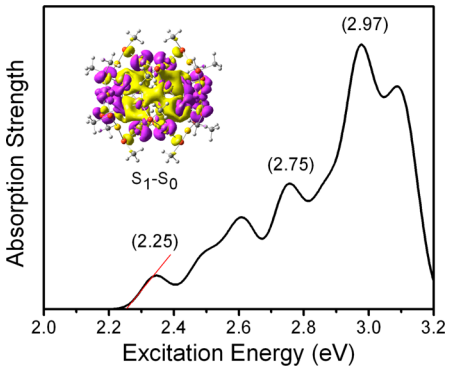

Figure 3. Theoretical optical absorption spectrum of $Au_{20}(SR)_{16}$ calculated by TD-DFT using the PBE function. The inset shows the CDD image of the S_1-S_0 transition, where purple represents hole density and yellow electron density.

the acceptor. It is known that the nature and degree of intramolecular charge transfer (ICT) are significantly influenced by their surrounding environments, where the solvation that arose from solute−solvent interactions could change the excited state charge transfer dynamics. To determine these properties, femtosecond transient absorption measurements can further provide the solvent-dependent dynamical information about the dynamics of the ICT state.

Femtosecond Transient Absorption Measurements. To unravel the exited state characteristics of $Au_{20}(SR)_{16}$ clusters and elucidate the solvent-dependent relaxation pathway, broadband femtosecond transient absorption measurements were taken using a 400 nm excitation. Figure 4 shows transient absorption spectra of $Au_{20}(SR)_{16}$ from 0 fs to 90 ps in toluene and THF. Generally, the transient absorption spectrum is comprised of broad excited state absorption (ESA, positive transient absorption signal) overlapping with ground state bleach (GSB) and stimulated emission (SE, negative transient absorption signal). In toluene, the broad ESA band shows two maxima around 550 and 720 nm over the whole measured time window (see Figure 4A). The dip at 480 nm is assigned to the ground state bleach (resembling the linear absorption spectrum) superimposed over the broad excited state absorption. A closer look at the initial transient absorption spectra found that a weak ESA signal around 465 nm rises shortly after excitation (within a 150 fs time delay) and decays rapidly to give rise to another ESA around 750 nm during the first picosecond, indicating the growth of a new transient state. A direct comparison of kinetic traces is shown in Figure S3 of the Supporting Information. From the kinetic decay traces, it is seen that the ESA around 480 nm decays rapidly with ESA around 625 and 745 nm rising simultaneously, which arise from an intermediate state. However, little change is observed in the intensity and shape of the overall spectrum in the next 90 ps. Global analysis is further employed to extract the time-independent correlations as the EADS from these transient absorption data.[27] As a result, the transient absorption spectrum of $Au_{20}(SR)_{16}$ in toluene is fit well using a sequential model with three components having decay times of 302 fs, 1 ps, and >1 ns (Figure 5A). To determine if the excitation power influences the excited state dynamics, transient absorption of $Au_{20}(SR)_{16}$ in toluene was measured with pump powers of ~200 and ~120 nJ/pulse (spot size of ~120 μm in each case); the spectra and dynamics indeed did not show any power dependence (see section S2 of the Supporting Information). Comparison of the EADS on different time scales shows that the majority of the spectral features of the first and second components are negatively correlated, e.g., the dip around 550 nm in the first component and the ESA around 550 nm in the second component. The spectrum of the first component (302

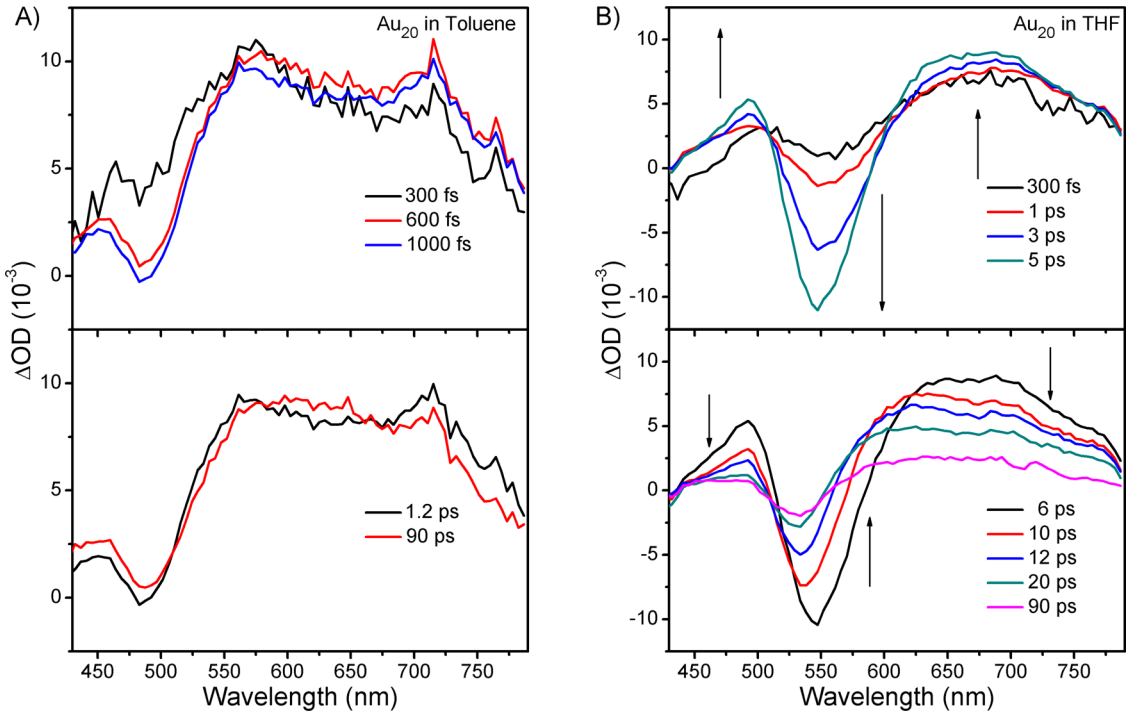

Figure 4. Evolution of the transient absorption spectra of the $Au_{20}(SR)_{16}$ cluster. The spectra of $Au_{20}(SR)_{16}$ dissolved in (A) toluene and (B) THF at different delay times (pump at 400 nm).

dx.doi.org/10.1021/jp406336q | J. Phys. Chem. A 2013, 117, 10294−10303

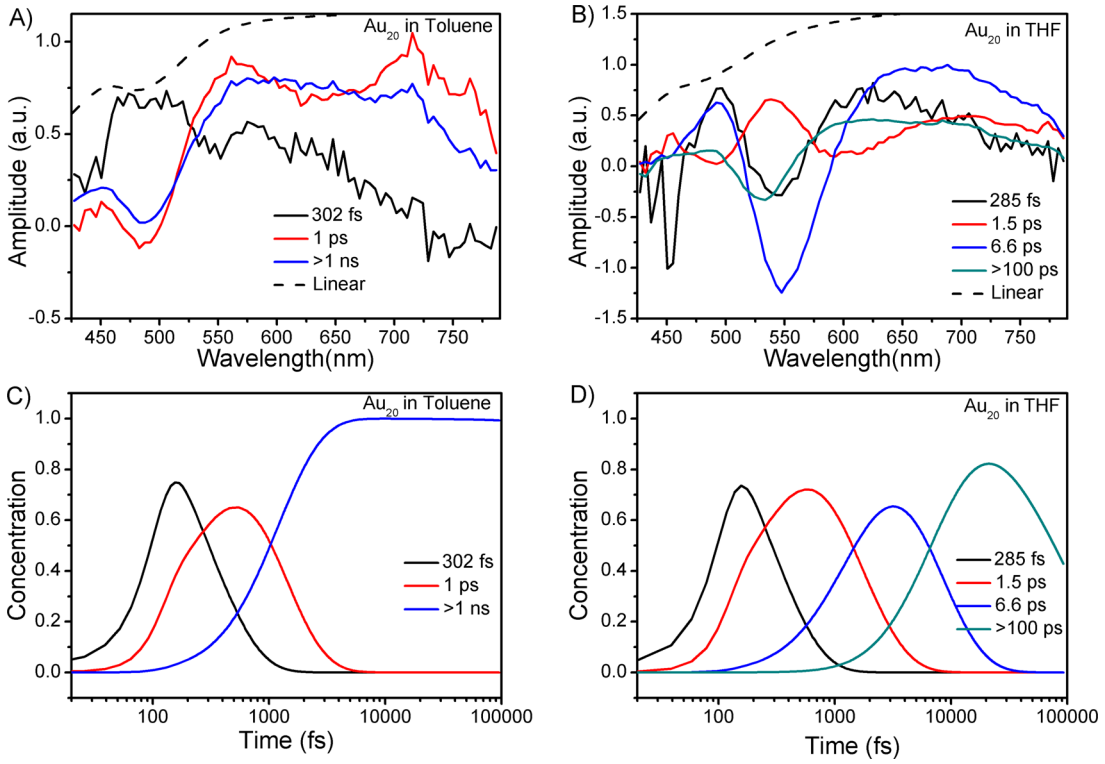

Figure 5. Global analysis of the transient absorption spectra. EADS obtained using a sequential relaxation model for $Au_{20}(SR)_{16}$ dissolved in (A) toluene and (B) THF. The linear absorption spectrum (———) is plotted on an arbitrary reverse vertical axis. Note that the lifetime of the last state was fixed to 1 ns and 100 ps in toluene and THF, respectively. Concentrations of the EADS components as a function of time in (C) toluene and (D) THF.

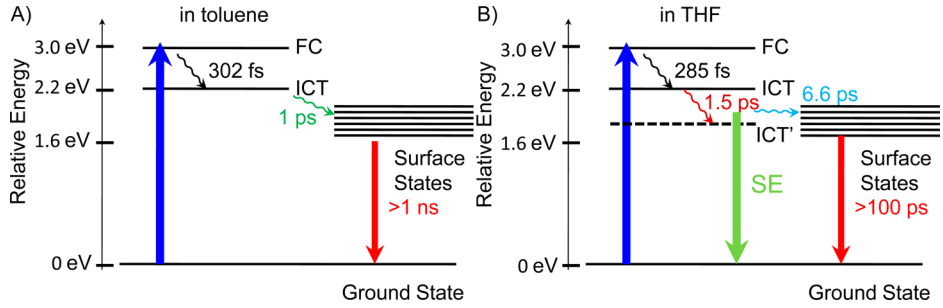

Figure 6. Relaxation pathway of $Au_{20}(SR)_{16}$ in toluene (A) and THF (B) based on global analysis. In more polar solvent THF, an ICT′ state emerges to yield the best global fitting. The recombination time of the electrons ranges from >1 ns in toluene to >100 ps in THF.

fs) composed by ESA with broad peaks between 460 and 520 nm is ascribed to the signal of the higher excited state (Franck–Condon state) populated by the 400 nm excitation. Subsequently, the second 1 ps component stands for the ICT state and displays strong ESA above 650 nm; the GSB contribution becomes evident at 480 nm because of the rapid decay of ESA in this spectral region. Compared with the 1 ps component, the GSB around 480 nm and ESA around 720 nm in the long-lived state (>1 ns) component show fast decay. This long lifetime state (>1 ns) commonly seen in semiconductor nanoparticles is herein attributed to the $Au_3(SR)_4$ semiring state or trap state, which can localize charge carriers and decelerate recombination.[12,38] Furthermore, the concentration kinetics are extracted and plotted in Figure 5C. It is obvious that the rise and decay of the EADS of $Au_{20}(SR)_{16}$ in toluene follow the sequential model during the relaxation; e.g., the second EADS rise with the first lifetime and decay with the second lifetime. The relaxation model of $Au_{20}(SR)_{16}$ in toluene is summarized in Figure 6A.

In contrast, entirely different transient absorption spectra are seen for $Au_{20}(SR)_{16}$ clusters dissolved in THF (Figure 4B). During the first 5 ps, stimulated emission is clearly observed around 550 nm, with the ESA around 500 nm gradually shifting to 480 nm and masking the GSB at this wavelength according to the steady state absorption spectrum. The blue shift of ESA typically results from the solvent-stabilized ICT state (denoted as ICT′), as solvation could gradually lower the excited state potential energy surface with delay time.[39,40] The presence of an ICT′ state can be further confirmed in the kinetic traces of THF, where the ESA at 480 and 675 nm rise slowly during the first 5 ps together with the stimulated emission around 550 nm simultaneously (see Figure S3 of the Supporting Information).

Compared to that in toluene, the transient absorption of $Au_{20}(SR)_{16}$ in THF determined by global analysis exhibits much more pronounced relaxation dynamics. As shown in

dx.doi.org/10.1021/jp406336q | J. Phys. Chem. A 2013, 117, 10294–10303

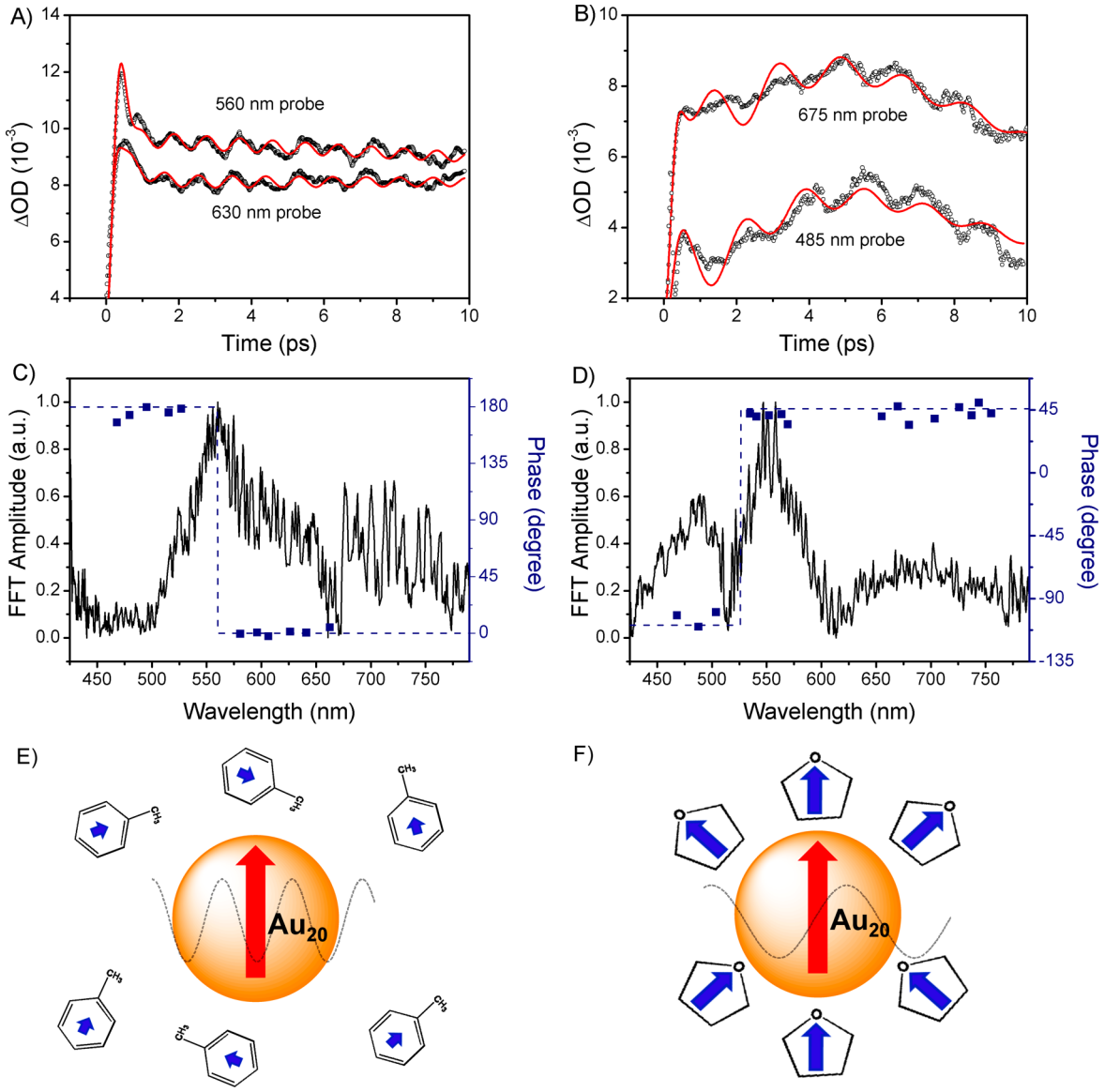

Figure 7. Representative kinetic traces (circles) and corresponding fitting traces (red lines) probed at 560 and 630 nm in toluene (A) and at 485 and 675 nm in THF (B), showing the solvent-dependent oscillations. Amplitude spectra (left axis) and phases (right axis) of the oscillations in toluene (C) and THF (D). Schematic illustrations of the relative positions of excited $Au_{20}(SR)_{16}$ clusters in toluene (E) and THF (F) molecules in which the red and blue arrows stand for dipoles of the clusters and solvent molecules, respectively.

Figure 5B, four components (285 fs and 1.5, 6.6, and >100 ps) are then required to obtain the best fit from the global analysis. The EADS of the first component (285 fs) shows ESA with two broad peaks around 500 and 640 nm, as well as a negative dip around 550 nm. Subsequently, the second component with ESA around 550 and 700 nm is from the ICT state together with a small GSB around 480 nm, in agreement with that observed in toluene. Similar to the case in toluene, the majority of spectral features of the first and second EADS components are negatively correlated. The ESA around 550 nm of the second component has a rise time associated with the buildup of carriers, which is represented by the negative amplitude in the spectra of the first component.[14] Therefore, the ESA peaks of the first component are ascribed to the signal of the higher excited state (Franck−Condon state) populated by the 400 nm excitation, whereas the dip around 550 nm is due to the mathematical correlation with the second component. The rapid decay of ESA (ICT) around 550 nm with a time constant of 1.5 ps (close to the solvation time of THF) is accompanied by a simultaneous rise of ESA around 480 and 675 nm, which is the typical sign of formation of the solvent-stabilized ICT (ICT′) state. This ICT′ state, which lasts for 6.6 ps, is followed by formation of the last long-lived surface state (>100 ps). Furthermore, during the first 20 ps upon excitation, the negative stimulated emission dip around 550 nm experiences a blue shift with time, obviously because of the spectral shift and broadening of the overlapped ESA of the ICT′ state formed during solvation and relaxation, which is dependent on solvent polarity. In toluene, because of the short-lived ICT state, the SE can hardly be seen around 550 nm and the blue shift cannot be clearly distinguished. This shift is clearly seen in the last EADS component with a subnanosecond decay of broad ESA, in contrast with much a slower decay in toluene. The resulting relaxation model of the excited $Au_{20}(SR)_{16}$ cluster in THF is summarized in Figure 6B.

dx.doi.org/10.1021/jp406336q | J. Phys. Chem. A 2013, 117, 10294−10303

For $Au_{20}(SR)_{16}$ in both toluene and THF, stimulated emission from the surface states can explain the dip in the transient absorption signal in the NIR spectral region that lasts until the end of the measurement. The ICT state in toluene lasts only 1 ps, leading to less stimulated emission from the ICT state around 550 nm hidden by the larger positive ESA signal. In THF, however, the solvent dipoles can be reorganized around the excited $Au_{20}(SR)_{16}$ cluster surface, which gradually decreases the energy of the ICT state and results in the formation of the ICT′ state. Thus, the ICT′ state energy could be equal to or slightly lower than the energy of the trap state to some extent so that the trapping of charge is slower (~6.6 ps) in THF than in toluene (1 ps), which causes relatively stronger visible luminescence in THF. This is why the stimulated emission around 550 nm in THF is stronger than that in toluene. On the basis of the results described above, it is suggested that the dual fluorescence of $Au_{20}(SR)_{16}$ in the visible and NIR regions arises from core states and long-lived surface states, respectively, that are localized on different energy surfaces.

Oscillatory Features. A careful examination of the wavelength-dependent transient kinetics shows that, as in the cases of other gold clusters of various sizes,[13,14,21,22] $Au_{20}(SR)_{16}$ clusters in both solvents exhibit prominent oscillatory features with different vibration periods at early times as shown in Figure 7. Because the solvation process has a significant impact on the dynamics of ICT states of excited $Au_{20}(SR)_{16}$, it is interesting to see whether the oscillatory features also exhibit any solvent-dependent characteristics. In both solvents, oscillations can be clearly seen at most wavelengths for transient kinetics. In less polar toluene, the Fourier transform of positive early time kinetic data gives a modulation frequency of 36 cm^{-1} (1.08 THz) (see Figure S4 of the Supporting Information), close to the calculated frequency of the vibration mode of the ground state around 39.6 cm^{-1} (1.2 THz) (the assignments of observed vibration modes are shown in section S4 of the Supporting Information). In more polar THF, however, a frequency of ~20 cm^{-1} (0.6 THz) is obtained from the Fourier transform of early time kinetic data. Such a large discrepancy in the oscillation frequency of $Au_{20}(SR)_{16}$ between toluene and THF, which may be related to solvent reorganization around the excited $Au_{20}(SR)_{16}$ cluster, has never been reported before in studies of Au clusters. To obtain the damping time and the phase information of the oscillations, a fitting procedure including convolution of the Gaussian impulsive function was used:[14,41]

$$\Delta A = A \exp(-t^2/2\sigma^2) \times [B \exp(-t/\tau_1) + C \exp(-t/\tau_2) \cos(\omega t + \phi) + D \exp(-t/\tau_3)]$$

where σ represents the standard deviation of the laser pulse, ω stands for the frequency of the oscillation, ϕ is the phase of the oscillation, τ_1 and τ_3 represent the excited state decay time constants, and τ_2 is the damping time, reflecting the lifetime of oscillation. In THF, an extra exponential decay in τ_4 from solvation was added to obtain the best fit. The resulting damping time is ~20 ps in toluene and 5 ps in THF, which is clearly solvent-dependent. Furthermore, at different probe wavelengths in the same solvent, it is found that the frequency and damping time of the oscillations are identical but the phases are prominently shifted (Figure 7C,D).

To gain deeper insight into the oscillation in $Au_{20}(SR)_{16}$ clusters, the Fourier transform of the early transients at each wavelength in these two solvents was performed to calculate the amplitude and phase spectra corresponding to the 36 cm^{-1} (1.08 THz) mode in toluene and the 20 cm^{-1} (0.62 THz) mode in THF (Figure 7C,D). It is known that the Fourier transform amplitude corresponds to the strength of coupling between the vibration mode and the electronic states. In toluene, we find that the amplitude of the oscillation peaks off-resonance with a low FT amplitude of ~0.1 in the region of 450−500 nm, where ESA and GSB overlap. On the other hand, in THF a distinct peak around 480 nm with a FT amplitude of ~0.58 is clearly seen from the amplitude spectrum, which is in agreement with the ESA of the ICT′ state around 480 nm shifted from 550 nm because of the solvation process in THF. Furthermore, as shown in Figure 7, all the oscillation peaks in FT amplitude spectra of $Au_{20}(SR)_{16}$ in both solvents exhibit strong antiresonance near the transition (ESA, GSB, and SE) boundaries, indicating that the transition energy rather than the overall transition amplitude is modulated.[14,15] Such antiresonance features can be further identified from the spectrally dependent phases of the oscillation in both solvents (Figure 7C,D).

The phase spectra show a pronounced π shift near the ESA peak (560 nm) in toluene and a $^3/_4\pi$ shift at the peak of stimulated emission (550 nm) in THF, suggesting that the energy level structure of the $Au_{20}(SR)_{16}$ cluster was modulated by a vibrational wavepacket.[42] Previous investigations of large gold nanoparticles showed that the phase of the oscillation had a π shift on different sides of the SPR peak because the periodic shift occurs in the position of the SPR due to the small periodic change in the particle volume caused by the acoustic vibration mode.[41,43] For $Au_{20}(SR)_{16}$ clusters in our investigation, a discrete, multiband absorption spectrum with a large HOMO−LUMO gap of 2.15 eV is seen. The optically excited vibrations of small size Au clusters in pump−probe measurements is explained well by the displacive excitation mechanism.[22,44] In the case of $Au_{20}(SR)_{16}$, a picture of displacive excitation coherent phonons of $Au_{20}(SR)_{16}$ can thus be drawn as follows: the nuclear motion was induced upon excitation through changing the equilibrium position of the nuclear position with respect to the ground state geometry of the $Au_{20}(SR)_{16}$ cluster,[45] which generated a wavepacket motion along the excited state potential energy surface. As the band gap emerges in $Au_{20}(SR)_{16}$, the excited state configuration lives long enough to maintain the new equilibrium positions for several periods of vibration. Changes in the particle size led by the vibration modify the electron density distribution and the band gap and thus modulate the transient absorption signals of $Au_{20}(SR)_{16}$ clusters. When moving along the potential energy surface, the wavepacket passes twice through its center, leading to a phase shift of oscillations on both sides of this region.[44,46]

To understand the solvation-dependent dynamics in excited $Au_{20}(SR)_{16}$, we then tried to draw the physical picture of the dynamical process involved for a solute [$Au_{20}(SR)_{16}$ cluster here] molecule in polar THF. Upon femtosecond excitation, an induced dipole in the excited $Au_{20}(SR)_{16}$ cluster is created at time zero, which gives rise to an instantaneous electric field on the polar solvent molecules. Subsequently, the solvent molecules begin to move and rearrange themselves by both steric and electrostatic effects around the excited $Au_{20}(SR)_{16}$ cluster surface to reach their new equilibrium positions.[40,47−49] As solvation proceeds, the energy of the excited $Au_{20}(SR)_{16}$ cluster gradually decreases, probably giving rise to a blue shift in the observed ESA spectrum. From Figure 2A, it is found that

there is no obvious shift in the absorption spectra, while in transient absorption spectra (Figure 4B), a blue-shifted ESA from 550 to 480 nm is clearly observed in THF, indicating the formation of the solvent-stabilized ICT′ state from the initial ICT state, where the potential energy surface of the excited ICT state gradually decreases during solvation. The appearance of the oscillation amplitude peak around 480 nm further confirms the formation of such a solvation-stabilized ICT state (ICT′) in THF as shown in Figure 7D. As a result, compared with less polar toluene, it is reasonable to expect that the more polar THF molecules are strongly rearranged and closely approach the excited $Au_{20}(SR)_{16}$ cluster surface, forming a single-layer solvent shell during the solvation (Figure 7E,F), leading to a larger oscillator mass that gives rise to a lower vibration frequency.

As mentioned above, it is found that the oscillation gives a frequency of 36 cm^{-1} in toluene, which is close to the calculated vibration mode of 39.6 cm^{-1}, whereas the frequency is largely reduced to 20 cm^{-1} in THF, indicating that solvation could play a significant role in modulating the observed oscillations because ICT dynamics is very sensitive to solvent polarity. In addition, toluene and THF have similar viscosities of ∼0.56 and ∼0.46 cP, respectively,[50] but compared to the low polarity (Δf) of ∼0.0159 and small dipole moment of 0.3 D of toluene, THF has a higher polarity (Δf) of up to 0.210 with a larger dipole moment of 1.8 D,[51,52] which suggests that it is the solvent polarity, rather than viscosity, that has a stronger impact on the excited state relaxation.[23]

With regard to the vibrations in transient absorption spectra of those larger Au nanoparticles with diameters in the range of 5−100 nm, much work examining different aspects has been conducted.[43,53−55] However, the mechanism of vibrations in very small metal clusters (e.g., <1 nm) is not very clear yet. For larger metal nanoparticles, electron−phonon coupling can well explain the transfer of energy from the electron system to the lattice, in which the electron−phonon relaxation is dependent on laser power.[54] On the other hand, very small $Au_{20}(SR)_{16}$ clusters exhibit power-independent relaxation, indicating that electron−phonon coupling is not operative in such systems.[18,19] The lack of laser power dependence on the cooling rate in $Au_{20}(SR)_{16}$ suggests that the ultrafast electron cooling is dominated. A previous study indicated that the oscillation frequency is independent of size for Au monolayer-protected clusters smaller than 2.2 nm and the frequency is 2.2 THz.[22] The observed oscillation frequency (∼1.08 THz) of $Au_{20}(SR)_{16}$ in toluene is lower than the previous value of 2.2 THz. Because the displacive coherent phonon excitation mechanism requires excitation of only modes that do not change the symmetry,[44] both the symmetric breathing modes of the Au_8 core and the Au−S−Au bending modes could be possibly observed. In our work (also see section S4 of the Supporting Information), when $Au_{20}(SR)_{16}$ is dissolved in toluene, we have observed a weaker breathing mode of the Au_8 core around 101.7 cm^{-1} of $Au_{20}(SR)_{16}$, and stronger 36 cm^{-1} (corresponding to the calculated 39.6 cm^{-1}) Au−S−Au bending modes through the Fourier transform. Furthermore, the 101.7 cm^{-1} mode is suppressed when $Au_{20}(SR)_{16}$ is dissolved in more polar THF, and only the 20 cm^{-1} mode in THF dominates, which may be shifted from the 36 cm^{-1} mode in toluene.

To our surprise, we have tried to observe the oscillation of $Au_{20}(SR)_{16}$ in nonpolar hexane to see the original breathing mode around 101.7 cm^{-1}, and there is no obviously distinguishable oscillation of $Au_{20}(SR)_{16}$ in nonpolar cyclohexane because of the very small size of the cluster. Because the oscillation becomes stronger as cluster size increases,[56] the intensity and period (time of one cycle) of the observed oscillation of $Au_{20}(SR)_{16}$ increase with an increased solvent polarity, indicating that the total cluster size of $Au_{20}(SR)_{16}$ is increased by attaching more polar solvents around the $Au_{20}(SR)_{16}$ cluster surface during solvation.

Besides, as the vibration frequency of $Au_{20}(SR)_{16}$ clusters is sensitive to the adsorbed solvents as shown above, it may act as a mass detector similar to those nanomechanical resonators.[57] Considering a harmonic oscillator model, the frequency of the oscillator with an effective mass of m_n can be calculated by[58]

$$\omega_n = \sqrt{k/m_n}$$

where k is elastic constant. As the vibration in $Au_{20}(SR)_{16}$ cluster is less influenced by solvent molecules in less polar toluene, we take the vibration frequency of the $Au_{20}(SR)_{16}$ cluster in toluene to be the original (intrinsic) frequency of the $Au_{20}(SR)_{16}$ oscillator. The total molar mass of THF molecules attached to the excited $Au_{20}(SR)_{16}$ cluster is thus roughly estimated to be ∼13735. Dividing by the molar mass of the THF molecule, we estimated that there are approximately 190 THF molecules adsorbed around an excited $Au_{20}(SR)_{16}$ cluster surface. Because toluene is not a complete nonpolar solvent, the results here actually show the mass difference between toluene and THF around $Au_{20}(SR)_{16}$ during the solvation. Thus, via combination of the oscillation frequencies in a series of solvents with different polarity, the solvation-dependent vibration of excited Au clusters in different environments may possibly act as a solvent mass sensor that may stimulate more related applications in the future. Investigations of the impact of solvation on vibration dynamics and energy exchange processes will provide deeper insight into the complicated spectral properties with different surrounding environments.

CONCLUSIONS

In conclusion, we have identified the intramolecular charge transfer (ICT) in excited $Au_{20}(SR)_{16}$ clusters, showing that the semiring ligands act as the donor of electron density and the Au_8 core acts as the electron acceptor. In more polar THF, an extra ICT′ state derived from ICT state is observed, leading to the final relaxation to the ground state that is accelerated >100-fold compared to that with the less polar toluene as the solvent. Moreover, the oscillations in $Au_{20}(SR)_{16}$ clusters are also observed in femtosecond transient absorption measurements and are attributed to modulations of the sample transmission caused by displacive excitation. The obvious discrepancy in oscillation frequency between THF and toluene results from the increased mass of the transient oscillator, where the more polar THF molecules are strongly attached to the excited $Au_{20}(SR)_{16}$ cluster surface due to stronger solvation, leading to the reduced oscillation frequency. By correlating the phonon frequencies of $Au_{20}(SR)_{16}$ in these two solvents, we can semiquantitatively estimate the mass or number of the surrounding solvent molecules (e.g., ∼190 THF molecules per excited Au_{20} cluster), which renders the observed oscillation a potential solvent molecule mass sensor. The results from our work, for the first time, provide insights for understanding the nature of ICT, the large influence of solvation on both the oscillatory feature and the excited state dynamics of monolayer-protected gold clusters.

dx.doi.org/10.1021/jp406336q | J. Phys. Chem. A 2013, 117, 10294−10303

■ ASSOCIATED CONTENT

Supporting Information

Steady state fluorescence measurement of neat solvents, additional spectra and dynamics, Fourier transform of oscillations, and details of quantum chemical calculations. This material is available free of charge via the Internet at http://pubs.acs.org.

■ AUTHOR INFORMATION

Corresponding Authors

*E-mail: andong@iccas.ac.cn.
*E-mail: guoqj@iccas.ac.cn.
*E-mail: rongchao@andrew.cmu.edu.

Notes

The authors declare no competing financial interest.

■ ACKNOWLEDGMENTS

S.V. is thankful for the support from the CAS Research Fellowship for International Young Researchers. This work was supported by NSFCs (21173235, 91233107, 21127003 and 21333012), the 973 Program (2013CB834604), and the Chinese Academy of Sciences.

■ REFERENCES

(1) Chen, S. W.; Ingram, R. S.; Hostetler, M. J.; Pietron, J. J.; Murray, R. W.; Schaaff, T. G.; Khoury, J. T.; Alvarez, M. M.; Whetten, R. L. Gold Nanoelectrodes of Varied Size: Transition to Molecule-like Charging. *Science* **1998**, *280*, 2098−2101.

(2) Qian, H.; Zhu, M.; Wu, Z.; Jin, R. Quantum Sized Gold Nanoclusters with Atomic Precision. *Acc. Chem. Res.* **2012**, *45*, 1470−1479.

(3) Turner, M.; Golovko, V. B.; Vaughan, O. P.; Abdulkin, P.; Berenguer-Murcia, A.; Tikhov, M. S.; Johnson, B. F.; Lambert, R. M. Selective Oxidation with Dioxygen by Gold Nanoparticle Catalysts Derived from 55-Atom Clusters. *Nature* **2008**, *454*, 981−983.

(4) Gao, L.; Jin, R. Atomically Precise Gold Nanoclusters as New Model Catalysts. *Acc. Chem. Res.* **2013**, *46*, 1749−1758.

(5) Hainfeld, J. F. A Small Gold-Conjucated Antibody Label: Improved Resolution for Electron-Microscopy. *Science* **1987**, *236*, 450−453.

(6) Wyrwas, R. B.; Alvarez, M. M.; Khoury, J. T.; Price, R. C.; Schaaff, T. G.; Whetten, R. L. The Colours of Nanometric Gold: Optical Response Functions of Selected Gold-Cluster Thiolates. *Eur. Phys. J. D* **2007**, *43*, 91−95.

(7) Ramakrishna, G.; Varnavski, O.; Kim, J.; Lee, D.; Goodson, T. Quantum-Sized Gold Clusters as Efficient Two-Photon Absorbers. *J. Am. Chem. Soc.* **2008**, *130*, 5032−5033.

(8) Link, S.; Beeby, A.; FitzGerald, S.; El-Sayed, M. A.; Schaaff, T. G.; Whetten, R. L. Visible to Infrared Luminescence from a 28-Atom Gold Cluster. *J. Phys. Chem. B* **2002**, *106*, 3410−3415.

(9) Jadzinsky, P. D.; Calero, G.; Ackerson, C. J.; Bushnell, D. A.; Kornberg, R. D. Structure of a Thiol Monolayer-Protected Gold Nanoparticle at 1.1 Angstrom Resolution. *Science* **2007**, *318*, 430−433.

(10) Heaven, M. W.; Dass, A.; White, P. S.; Holt, K. M.; Murray, R. W. Crystal structure of the gold nanoparticle $[N(C_8H_{17})_4][Au_{25}(SCH_2CH_2Ph)_{18}]$. *J. Am. Chem. Soc.* **2008**, *130*, 3754−3755.

(11) Wang, G. L.; Huang, T.; Murray, R. W.; Menard, L.; Nuzzo, R. G. Near-IR Luminescence of Monolayer-Protected Metal Clusters. *J. Am. Chem. Soc.* **2005**, *127*, 812−813.

(12) Kuno, M.; Lee, J. K.; Dabbousi, B. O.; Mikulec, F. V.; Bawendi, M. G. The Band Edge Luminescence of Surface Modified CdSe Nanocrystallites: Probing the Luminescing State. *J. Chem. Phys.* **1997**, *106*, 9869−9882.

(13) Miller, S. A.; Womick, J. M.; Parker, J. F.; Murray, R. W.; Moran, A. M. Femtosecond Relaxation Dynamics of $Au_{25}L_{18}^-$ Monolayer-Protected Clusters. *J. Phys. Chem. C* **2009**, *113*, 9440−9444.

(14) Sfeir, M. Y.; Qian, H.; Nobusada, K.; Jin, R. Ultrafast Relaxation Dynamics of Rod-Shaped 25-Atom Gold Nanoclusters. *J. Phys. Chem. C* **2011**, *115*, 6200−6207.

(15) Qian, H.; Sfeir, M. Y.; Jin, R. Ultrafast Relaxation Dynamics of $[Au_{25}(SR)_{18}]^q$ Nanoclusters: Effects of Charge State. *J. Phys. Chem. C* **2010**, *114*, 19935−19940.

(16) Walter, M.; Akola, J.; Lopez-Acevedo, O.; Jadzinsky, P. D.; Calero, G.; Ackerson, C. J.; Whetten, R. L.; Groenbeck, H.; Hakkinen, H. A Unified View of Ligand-Protected Gold Clusters as Superatom Complexes. *Proc. Natl. Acad. Sci. U.S.A.* **2008**, *105*, 9157−9162.

(17) Devadas, M. S.; Kim, J.; Sinn, E.; Lee, D.; Goodson, T., III; Ramakrishna, G. Unique Ultrafast Visible Luminescence in Monolayer-Protected Au_{25} Clusters. *J. Phys. Chem. C* **2010**, *114*, 22417−22423.

(18) Yau, S. H.; Varnavski, O.; Gilbertson, J. D.; Chandler, B.; Ramakrishna, G.; Goodson, T., III Ultrafast Optical Study of Small Gold Monolayer Protected Clusters: A Closer Look at Emission. *J. Phys. Chem. C* **2010**, *114*, 15979−15985.

(19) Yau, S. H.; Varnavski, O.; Goodson, T., III An Ultrafast Look at Au Nanoclusters. *Acc. Chem. Res.* **2013**, *46*, 1506−1516.

(20) Dermota, T. E.; Zhong, Q.; Castleman, A. W. Ultrafast Dynamics in Cluster Systems. *Chem. Rev.* **2004**, *104*, 1861−1886.

(21) Varnavski, O.; Ramakrishna, G.; Kim, J.; Lee, D.; Goodson, T. Critical Size for the Observation of Quantum Confinement in Optically Excited Gold Clusters. *J. Am. Chem. Soc.* **2010**, *132*, 16−17.

(22) Varnavski, O.; Ramakrishna, G.; Kim, J.; Lee, D.; Goodson, T., III Optically Excited Acoustic Vibrations in Quantum-Sized Monolayer-Protected Gold Clusters. *ACS Nano* **2010**, *4*, 3406−3412.

(23) Pelton, M.; Tang, Y.; Bakr, O. M.; Stellacci, F. Long-Lived Charge-Separated States in Ligand-Stabilized Silver Clusters. *J. Am. Chem. Soc.* **2012**, *134*, 11856−11859.

(24) Wu, Z.; Jin, R. On the Ligand's Role in the Fluorescence of Gold Nanoclusters. *Nano Lett.* **2010**, *10*, 2568−2573.

(25) Glasbeek, M.; Zhang, H. Femtosecond Studies of Solvation and Intramolecular Configurational Dynamics of Fluorophores in Liquid Solution. *Chem. Rev.* **2004**, *104*, 1929−1954.

(26) Zhu, M.; Qian, H.; Jin, R. Thiolate-Protected Au_{20} Clusters with a Large Energy Gap of 2.1 eV. *J. Am. Chem. Soc.* **2009**, *131*, 7220−7221.

(27) van Wilderen, L. J. G. W.; Lincoln, C. N.; van Thor, J. J. Modelling Multi-Pulse Population Dynamics from Ultrafast Spectroscopy. *PLoS One* **2011**, *6*, e17373.

(28) van Stokkum, I. H. M.; Larsen, D. S.; van Grondelle, R. Global and Target Analysis of Time-Resolved Spectra. *Biochim. Biophys. Acta* **2004**, *1657*, 82−104.

(29) Perdew, J. P.; Burke, K.; Ernzerhof, M. Generalized Gradient Approximation Made Simple. *Phys. Rev. Lett.* **1996**, *77*, 3865−3868.

(30) Frisch, M. J.; Trucks, G. W.; Schlegel, H. B.; Scuseria, G. E.; Robb, M. A.; Cheeseman, J. R.; Scalmani, G.; Barone, V.; Mennucci, B.; Petersson, G. A.; et al. *Gaussian 03*, revision E.01; Gaussian, Inc.: Wallingford, CT, 2004.

(31) Pei, Y.; Gao, Y.; Shao, N.; Zeng, X. C. Thiolate-Protected $Au_{20}(SR)_{16}$ Cluster: Prolate Au_8 Core with New $Au_3(SR)_4$ Staple Motif. *J. Am. Chem. Soc.* **2009**, *131*, 13619−13621.

(32) Zhu, M.; Aikens, C. M.; Hollander, F. J.; Schatz, G. C.; Jin, R. Correlating the Crystal Structure of a Thiol-Protected Au_{25} Cluster and Optical Properties. *J. Am. Chem. Soc.* **2008**, *130*, 5883−5885.

(33) Lee, D.; Donkers, R. L.; Wang, G. L.; Harper, A. S.; Murray, R. W. Electrochemistry and Optical Absorbance and Luminescence of Molecule-like Au_{38} Nanoparticles. *J. Am. Chem. Soc.* **2004**, *126*, 6193−6199.

(34) Persson, N. K.; Sun, M. T.; Kjellberg, P.; Pullerits, T.; Inganas, O. Optical Properties of Low Band Gap Alternating Copolyfluorenes for Photovoltaic Devices. *J. Chem. Phys.* **2005**, *123*, 204718.

(35) Sun, M. T.; Kjellberg, P.; Ma, F. C.; Pullerits, T. Excited State Properties of Acceptor-Substitute Carotenoids: 2D and 3D Real-Space Analysis. *Chem. Phys. Lett.* **2005**, *401*, 558−564.

(36) Sun, M. T. Control of Structure and Photophysical Properties by Protonation and Subsequent Intramolecular Hydrogen Bonding. *J. Chem. Phys.* **2006**, *124*, 054903.
(37) Wan, Y.; Yan, L.; Zhao, Z.; Ma, X.; Guo, Q.; Jia, M.; Lu, P.; Ramos-Ortiz, G.; Luis Maldonado, J.; Rodriguez, M.; Xia, A. Gigantic Two-Photon Absorption Cross Sections and Strong Two-Photon Excited Fluorescence in Pyrene Core Dendrimers with Fluorene/Carbazole as Dendrons and Acetylene as Linkages. *J. Phys. Chem. B* **2010**, *114*, 11737−11745.
(38) Bawendi, M. G.; Wilson, W. L.; Rothberg, L.; Carroll, P. J.; Jedju, T. M.; Steigerwald, M. L.; Brus, L. E. Electronic-Structure and Photoexcited-Carrier Dynamics in Nanometer-Size CdSe Clusters. *Phys. Rev. Lett.* **1990**, *65*, 1623−1626.
(39) Ramakrishna, G.; Goodson, T., III Excited-State Eeactivation of Branched Two-Photon Absorbing Chromophores: A Femtosecond Transient Absorption Investigation. *J. Phys. Chem. A* **2007**, *111*, 993−1000.
(40) Pal, S. K.; Zewail, A. H. Dynamics of Water in Biological Recognition. *Chem. Rev.* **2004**, *104*, 2099−2123.
(41) Hartland, G. V. Coherent Vibrational Motion in Metal Particles: Determination of the Vibrational Amplitude and Excitation Mechanism. *J. Chem. Phys.* **2002**, *116*, 8048−8055.
(42) Sagar, D. M.; Cooney, R. R.; Sewall, S. L.; Dias, E. A.; Barsan, M. M.; Butler, I. S.; Kambhampati, P. Size Dependent, State-Resolved Studies of Exciton-Phonon Couplings in Strongly Confined Semiconductor Quantum Dots. *Phys. Rev. B* **2008**, *77*, 235321.
(43) Hartland, G. V. Optical Studies of Dynamics in Noble Metal Nanostructures. *Chem. Rev.* **2011**, *111*, 3858−3887.
(44) Zeiger, H. J.; Vidal, J.; Cheng, T. K.; Ippen, E. P.; Dresselhaus, G.; Dresselhaus, M. S. Theory for Displacive Excitation of Coherent Phonons. *Phys. Rev. B* **1992**, *45*, 768−778.
(45) Kelley, A. M. Electron-Phonon Coupling in CdSe Nanocrystals from an Atomistic Phonon Model. *ACS Nano* **2011**, *5*, 5254−5262.
(46) Dimitrov, S. D.; Dooley, C. J.; Trifonov, A. A.; Fiebig, T. Femtosecond Probing of Optical Phonon Dynamics in Quantum-Confined CdTe Nanocrystals. *J. Phys. Chem. C* **2009**, *113*, 4198−4201.
(47) Bagchi, B. Dynamics of Solvation and Charge-Transfer Reactions in Dipolar Liquids. *Annu. Rev. Phys. Chem.* **1989**, *40*, 115−141.
(48) Fleming, G. R.; Cho, M. H. Chromophore-Solvent Dynamics. *Annu. Rev. Phys. Chem.* **1996**, *47*, 109−134.
(49) Bagchi, B.; Biswas, R. Polar and Nonpolar Solvation Dynamics, Ion Diffusion, and Vibrational Relaxation: Role of Biphasic Solvent Response in Chemical Dynamics. *Adv. Chem. Phys.* **1999**, *109*, 207−433.
(50) Lide, D. R. *CRC Handbook of Chemistry and Physics*, 85th ed.; CRC Press: Boca Raton, FL, 2004.
(51) Horng, M. L.; Gardecki, J. A.; Papazyan, A.; Maroncelli, M. Subpicosecond Measurements of Polar Solvation Dynamics Coumarin 153 Revisited. *J. Phys. Chem.* **1995**, *99*, 17311−17337.
(52) Lippert, E. Spektroskopische Bestimmung des Dipolmomentes aromatischer Verbindungen im ersten angeregten Singulettzustand. *Z. Elektrochem.* **1957**, *61*, 962−975.
(53) Link, S.; El-Sayed, M. A. Optical Properties and Ultrafast Dynamics of Metallic Nanocrystals. *Annu. Rev. Phys. Chem.* **2003**, *54*, 331−366.
(54) Hartland, G. V. Coherent Excitation of Vibrational Modes in Metallic Nanoparticles. *Annu. Rev. Phys. Chem.* **2006**, *57*, 403−430.
(55) Voisin, C.; Del Fatti, N.; Christofilos, D.; Vallee, F. Ultrafast Electron Dynamics and Optical Nonlinearities in Metal Nanoparticles. *J. Phys. Chem. B* **2001**, *105*, 2264−2280.
(56) Tlahuice-Flores, A.; Whetten, R. L.; Jose-Yacaman, M. Vibrational Normal Modes of Small Thiolate-Protected Gold Clusters. *J. Phys. Chem. C* **2013**, *117*, 12191−12198.
(57) Barton, R. A.; Ilic, B.; Verbridge, S. S.; Cipriany, B. R.; Parpia, J. M.; Craighead, H. G. Fabrication of a Nanomechanical Mass Sensor Containing a Nanofluidic Channel. *Nano Lett.* **2010**, *10*, 2058−2063.
(58) Lassagne, B.; Garcia-Sanchez, D.; Aguasca, A.; Bachtold, A. Ultrasensitive Mass Sensing with a Nanotube Electromechanical Resonator. *Nano Lett.* **2008**, *8*, 3735−3738.